buildings

MDPI

Article

Experimental Investigation on Pure Torsion Behavior of Concrete Beams Reinforced with Glass Fiber-Reinforced Polymer Bars

Haoyang Bai, Jiafei Jiang *, Weichen Xue * and Xiang Hu

College of Civil Engineering, Tongji University, Shanghai 200092, China; baihaoyang@tongji.edu.cn (H.B.); hu_xiang@tongji.edu.cn (X.H.)

* Correspondence: jfjiang@tongji.edu.cn (J.J.); xuewc@tongji.edu.cn (W.X.)

Abstract: The failure mechanism of torsional concrete beams with fiber-reinforced polymer (FRP) bars is essential for developing the design method. However, limited experimental research has been conducted on the torsion behavior of concrete beams with FRP bars. Therefore, the pure torsion test of four large-scale FRP-RC beams (2800 mm × 400 mm × 200 mm) was conducted to investigate the influence of the stirrup ratio (0, 0.49%, and 0.98%) and longitudinal reinforcement ratio (3.01%, 4.25%) on torsion behavior. The test results indicated that three typical failure patterns, including concrete cracking failure, stirrup rupturing failure, and concrete crushing failure, were observed in specimens without stirrups (stirrup ratio 0), partially over-reinforced specimens (stirrup ratio 0.49%), and over-reinforced specimens (stirrup ratio 0.98%), respectively. The tangent angle of spiral cracks at the midpoint of the long side of the cross-section was approximately 45° initially for all specimens. The torque–twist angle curves exhibited a linear and bilinear behavior for specimens without stirrups and specimens with stirrups, respectively. As the stirrup ratio increased from 0 to 0.98%, torsion capacity increased from 24.9 kN·m to 27.8 kN·m, increased by 12%, ultimate twist angle increased from 0.0018 rad/m to 0.0403 rad/m. As the longitudinal reinforcement ratio increased from 3.01% to 4.25%, the torsion capacity increased from 27.8 kN·m to 28.3 kN·m, and the ultimate twist angle decreased from 0.0403 rad/m to 0.0244 rad/m. Based on test results, the stirrup strain limit of 5200 με and spiral crack angle of 45° was suggested for torsion capacity calculation. In addition, based on the database of torsion tests, the performance of torsion capacity provisions was assessed.

Keywords: fiber-reinforced polymer; concrete beam; torsion test; torsion capacity; failure pattern; spiral crack angle

Citation: Bai, H.; Jiang, J.; Xue, W.; Hu, X. Experimental Investigation on Pure Torsion Behavior of Concrete Beams Reinforced with Glass Fiber-Reinforced Polymer Bars. *Buildings* **2024**, *14*, 2617. https://doi.org/10.3390/buildings14092617

Academic Editors: Eugeniusz Koda, Duc-Kien Thai, Yiyi Zhou and Zhengyi Kong

Received: 9 July 2024
Revised: 15 August 2024
Accepted: 21 August 2024
Published: 23 August 2024

1. Introduction

Corrosion of steel reinforcement is one of the main factors for the deterioration of concrete structures. The corrosion problem has found an innovative solution in the form of substituting steel reinforcement with fiber-reinforced polymer (FRP) reinforcement in concrete structures [1]. Due to characteristics of high tensile strength, corrosion resistance, high specific strength (strength-to-weight ratio), etc., FRP bars have been increasingly applied in concrete structures subjected to harsh environments [2,3]. In FRP-reinforced concrete structures, FRP reinforcement can be divided into longitudinal FRP reinforcement and transverse FRP reinforcement (i.e., FRP stirrups). FRP longitudinal reinforcement mainly provides flexural resistance, while FRP stirrups mainly provide torsional and shear resistance. Regarding the mechanical properties of FRP stirrups, studies have shown that rupture of FRP stirrups occurs at the bend generally, and the tensile strength of FRP stirrups at the bend is less than the tensile strength of straight portion, typically about 40% of the tensile strength of straight portion [4]. The specific value of the tensile strength of the stirrup to the tensile strength of the straight portion ratio (i.e., strength retention rate) is mainly related to the ratio of the bend radius to stirrup diameter. Such a feature determines the

diverse behavior of concrete beams reinforced with FRP stirrups compared with that of steel-reinforced concrete beams (steel-RC beams).

The torsion behavior of steel-RC beams was investigated experimentally in terms of stirrup ratio and concrete strength [5–7]. Some researchers conducted studies on the influence of stirrup ratio on the torsion behavior of fiber-reinforced polymer bars reinforced concrete (FRP-RC) beams. In 2016, Benmokrane et al. [8,9] conducted an early investigation on the torsion behavior of GFRP-RC beams (4000 mm × 600 mm × 250 mm). The stirrup ratios varied from 0% to 0.94%. The test results showed that the specimen without stirrups experienced concrete cracking failure. For specimens with a stirrup ratio between 0.19% and 0.47%, stirrups rupture occurred at the bend. For the specimen with a stirrup ratio of 0.94%, concrete crushing failure occurred. Overall, increasing the stirrup ratio improved torsion capacity. The stirrup ratio increasing 5 times resulted in 1.8 times torsion capacity. Benmokrane et al. [9,10] also conducted a torsion test on CFRP-RC beams. The conclusions were similar to those for GFRP-RC beams. Three typical failure patterns—concrete cracking failure, stirrup rupturing failure, and concrete crushing failure—were realized. A fivefold increase in the CFRP stirrup ratio resulted in a 90% increase in torsion capacity. In 2020, Hadhood et al. [11] investigated the type of transverse reinforcement (rectangular spiral and stirrup) and spiral ratio effect on the torsion behavior of GFRP-RC beams. The results displayed that torsion capacity increased with the stirrup ratio. The torsion capacity of the specimens with GFRP spirals was 16% higher than that of the specimen with rectangular GFRP stirrups, attributed to the confinement of spirals and direct resistance of the crack opening with the stirrup leg perpendicular to the diagonal cracks [12]. They further concluded that with spiral ratios ranging from 0 to 0.89%, the torsion capacity increased by 160%. Additionally, some researchers conducted experimental studies on the torsion behavior of FRP-RC beams, focusing on concrete types, cross-section types, and stirrup types [13–16]. Summarily, the torsion behavior of FRP-RC beams differs from that of steel-RC beams, due to different bond behavior and mechanical properties of reinforcement [17]. However, there are few studies on pure torsion tests of FRP-RC beams, which exhibited little information on the spiral crack angle, crack width, and torque–twist angle behavior. Besides, the effect of longitudinal reinforcement has not been investigated. At last, stacked rollers were used as torsion support for all existing tests which could cause the specimens to twist around the rollers rather than around the center of the specimen's cross-section, changing the true stress state of the specimens and resulting in additional torque.

In terms of tensile strength of stirrups, CSA S6:19 [18], ACI 440.1R-15 [19], AASHTO GFRP-RC 2018 [20], and GB 50608-2020 [21] specify the stirrup strain limit as 4000 με. ACI 440.11-22 [22] and CSA S806-12 [23] specify the stirrup strain limit as 5000 με, which was derived from the shear behavior of FRP-RC beams. However, since the stress state of the stirrup legs in shear members and torsion members differed, the stirrup strain limit should be investigated for FRP-RC members under torsion specifically. Benmokrane et al. [8,10] conducted a comparative analysis based on the test results of GFRP and CFRP-RC beams. The study compared the differences between calculated torsion capacity using different tensile strengths of the FRP stirrup (test value of tensile strength of FRP stirrup at bend: $f_{bend,exp}$; 0.4 times the tensile strength of FRP stirrup of straight portion: $0.4 \cdot f_{fu}$; tensile strength corresponding to the stirrup strain limit ε_{lim} of 5000 με: $0.005 \cdot E_f$) and the test results. The results revealed that using $f_{bend,exp}$ to calculate the torsion capacity of GFRP and CFRP-RC members yielded results closest to the experimental results, with an error of about 4%. However, the conclusion relies on the equation from CSA S806-12. The tensile strength or strain limit of the stirrup still needs investigation.

From the above literature review, the following issues can be summarized:

1. In a few existing torsion tests of FRP-RC members, some points could be improved. For instance, stacked rollers were also used as a torsion support which could cause additional torque. The longitudinal reinforcement was arranged asymmetrically on the cross-section, resulting in uneven stress distribution in the longitudinal bars of

the upper and lower chords of the truss. The crack width and short legs of the stirrup were not measured.

2. Stirrup strain limit and spiral crack angles were summarized and analyzed to provide a suggestion for torsion capacity prediction.
3. A database for torsion tests of FRP-RC members was established and provided to assess the current torsion design provisions.

In this paper, a novel torsion support was designed and fabricated which was suitable for large-scale torsion tests of structural components and could allow the specimens to rotate around the center of the cross-section. This paper conducted a torsion test of four large-scale GFRP-RC beams (2800 mm × 400 mm × 200 mm) reinforced with symmetric longitudinal reinforcement including one specimen without stirrups, and the other three specimens with the variation of stirrup ratio and longitudinal ratio. The influence of longitudinal and transverse reinforcement ratio on the beam's torsion behavior in terms of failure pattern, spiral crack angle, torque–twist angle curve, strain development in reinforcement, concrete strut, etc., was investigated. Based on test results, the stirrup strain limit was suggested for torsion design. In addition, based on the database of torsion tests, the performance of torsion capacity provisions was assessed and the spiral crack angle was suggested for torsion design.

2. Experimental Program

2.1. Test Specimens

Four large-scale GFRP-RC beams with a total length of 2800 mm were designed according to codes CSA S806-12, ACI 440.1R-15, and GB 50608-2020 (as shown in Figure 1). The torsion span was kept constant at 1800 mm in the middle of the beams. The torsion span consisted of one 800 mm long test section in the middle of the torsion span and two 500 mm long stirrups-reinforced sections at both ends. On each side of the beams, an extra 500 mm length anchorage section was set to avoid bond failure before torsion failure. Besides, all beams were equipped with overhanging arms perpendicular to the longitudinal direction associated with the torsion setup. This design allowed the vertical load to be applied to the overhanging arms, enabling torque loading on the main section of the beams.

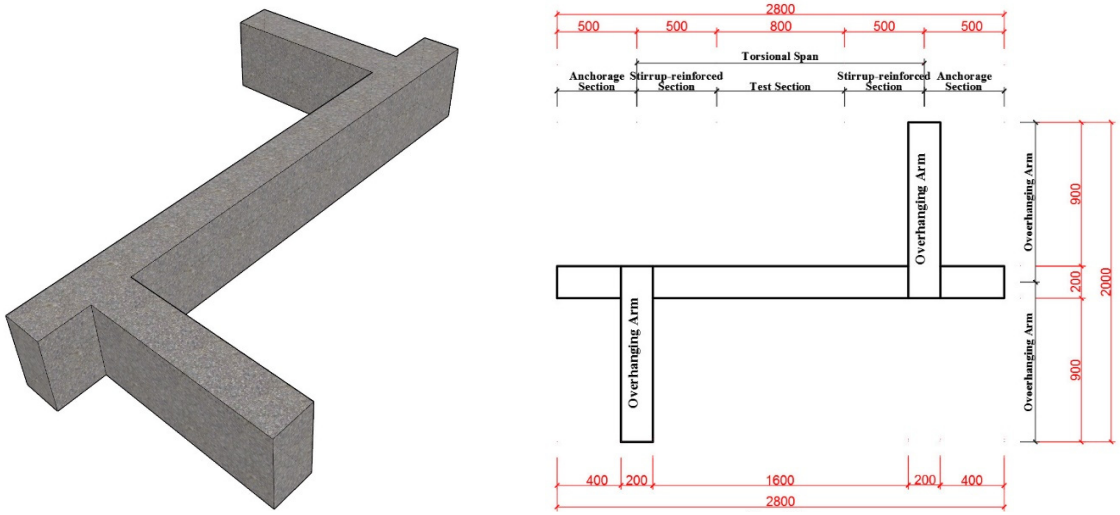

(**a**) (**b**)

Figure 1. *Cont.*

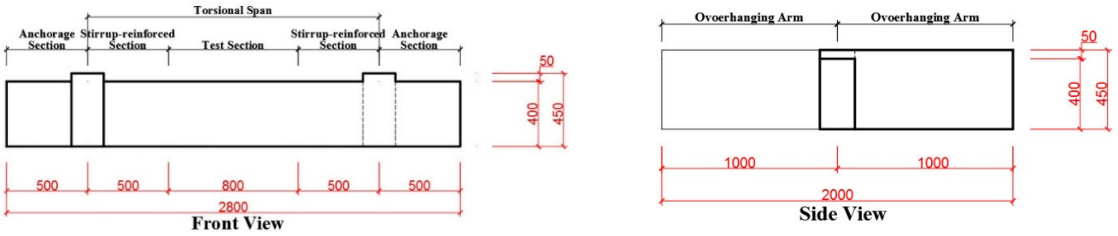

(**c**) (**d**)

Figure 1. Dimensions of specimens: (**a**) 3D diagram; (**b**) side view; (**c**) front view; (**d**) side view.

Four GFRP-RC beams are categorized into three types of specimens: specimen without stirrups (G-W-12D16-T), partially over-reinforced specimen (G-160-12D16-T), and over-reinforced specimen (G-80-12D16-T, G-80-12D19-T) (as listed in Table 1). The longitudinal reinforcement ratio ρ_l of the specimen without stirrups and the partially over-reinforced specimens was 3.01%. The two over-reinforced specimens had longitudinal reinforcement ratios of 3.01% and 4.25%, respectively. All specimens were reinforced with the longitudinal FRP bars symmetrically on the cross-section. The reinforcement details are illustrated in Figure 2.

Table 1. Specimen design details.

Specimens	Specimen Type	f_c' (MPa)	Stirrup Ratio ρ_t	Longitudinal Reinforcement Ratio ρ_l
G-W-12D16-T	Without stirrups	39	0	3.01%
G-160-12D16-T	Partially over-reinforced	39	0.49%	3.01%
G-80-12D16-T	Over-reinforced	42	0.98%	3.01%
G-80-12D19-T	Over-reinforced	41	0.98%	4.25%

The specimens were denoted with acronyms consisting of letters and numbers, indicating various test parameters. The first letter "G" designated GFRP. The second letter or number represented the type and quantity of stirrups ("W" for without stirrups and "80" for 80 mm spacing GFRP stirrups in the test section). The third letter with a number represented the configuration of longitudinal reinforcement ("12" or "6" for the number of longitudinal GFRP bars, "D16" or "D19" for the diameter of longitudinal GFRP bars). The last letter "T" indicated torque loading.

2.2. Material Properties

All specimens were cast using the target cylinder compressive strength of 40 MPa. The concrete compressive strength was tested according to the Chinese standard GB/T 50081 [24]. The corresponding cylinder concrete compressive strength f_c' (80% of the cube strength) is listed in Table 1. No. 16 and No. 19 GFRP reinforcements were used as longitudinal reinforcement, and No. 10 GFRP reinforcement was used as GFRP stirrups where the internal bend radius r_b was 30 mm. The tensile strength of the longitudinal GFRP reinforcements and GFRP stirrups were tested according to ACI 440.3R-12 [25]. The detailed material properties are listed in Table 2.

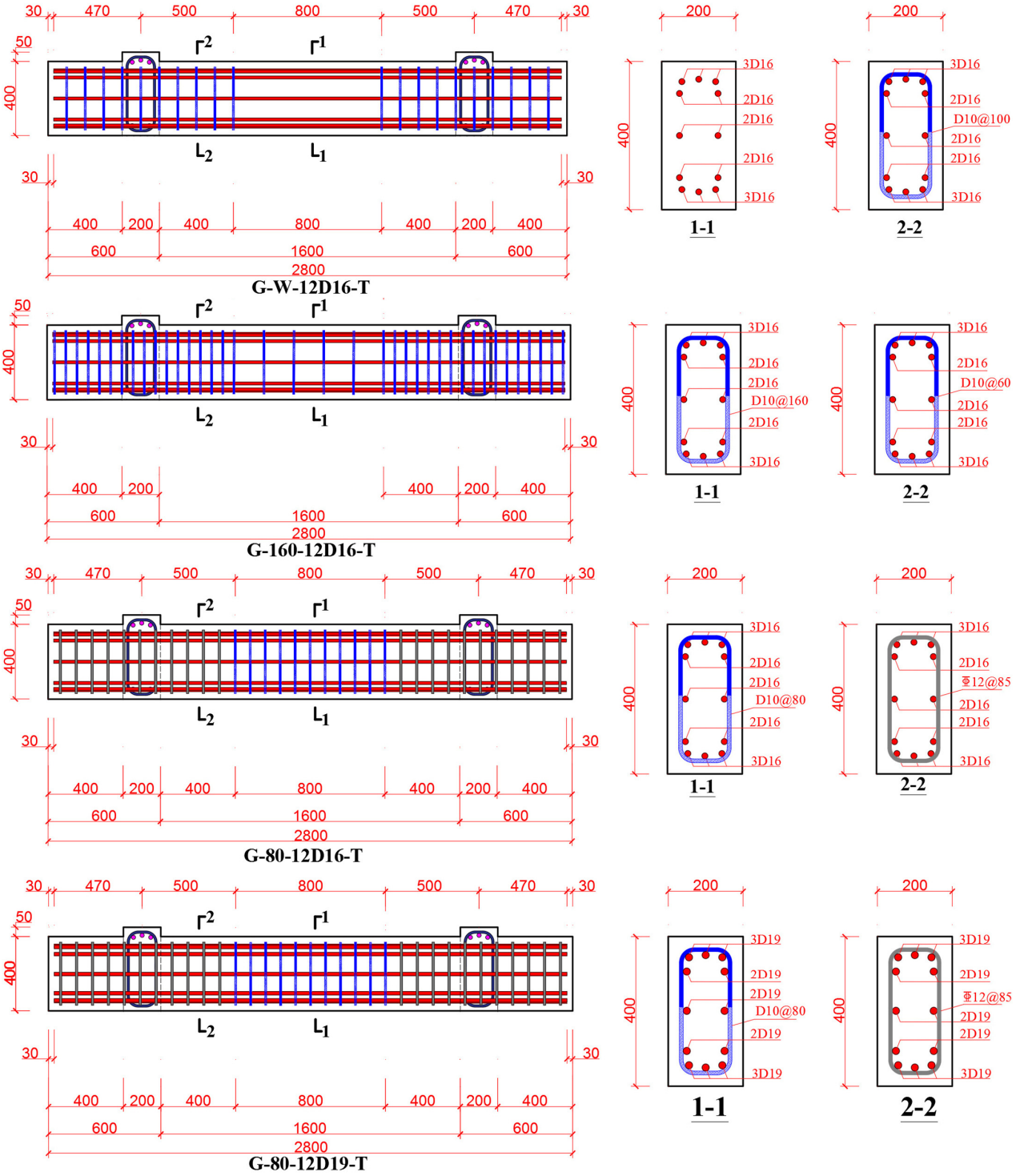

Figure 2. Reinforcement details of specimens.

Table 2. Mechanical properties of reinforcement.

Reinforcement	Nominal Diameter (mm)	Ultimate Strength (MPa)	Bend Strength (MPa)	Elastic Modulus (GPa)
No. 16 GFRP	16	1050	-	62
No. 19 GFRP	19	1090	-	60
No. 10 GFRP	10	1100	486	56

2.3. Test Setup

2.3.1. Loading Mode

The specimens were tested in the Building Structure Laboratory of Tongji University by using a specially designed and fabricated torsion test setup, as shown in Figure 3. The specimens were supported by two torsion supports. During the installation of the specimen, the cross-section center of the specimen coincided with the center of the torsion support to ensure specimens twisted around the center of the cross-section. Two 50-ton electro-hydraulic servo actuators were applied on the overhanging arms to apply torque to the specimens. Both actuators were connected to the same loading system.

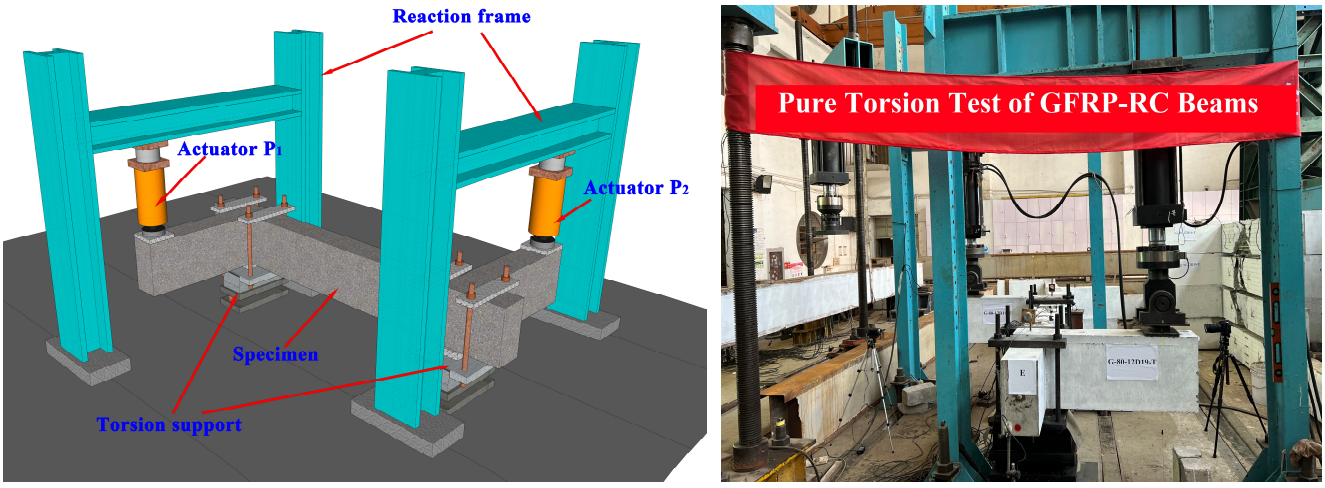

Figure 3. Test setup.

2.3.2. Torsion Support

A torsion support was designed and fabricated for torsion and combined torsion test specially (as shown in Figure 4). This torsion support had been applied for a patent [26]. The torsion support could provide the specimen with freedom of torsion, axial tension, and bending under torsional loads. The features of the torsion support could be summarized as follows:

1. To ensure that the specimens could twist around the center of the cross-section, adjustable height pads were placed between the beam and the lower clamp plate (pad thickness $t = R - 0.5h$, h: the height of cross-section, R: the radius of the upper curved support).
2. To reduce the friction caused by torsion, sliding rollers were installed on the upper and lower curved supports.
3. The anti-slip bolts could be installed on the upper and lower steel plates to prevent the rollers from sliding out during the test. Besides, two sets of key slots and raised circular discs were installed on the upper and lower steel plates and rollers respectively to ensure that the rollers could roll between the upper and lower steel plates in the same direction.

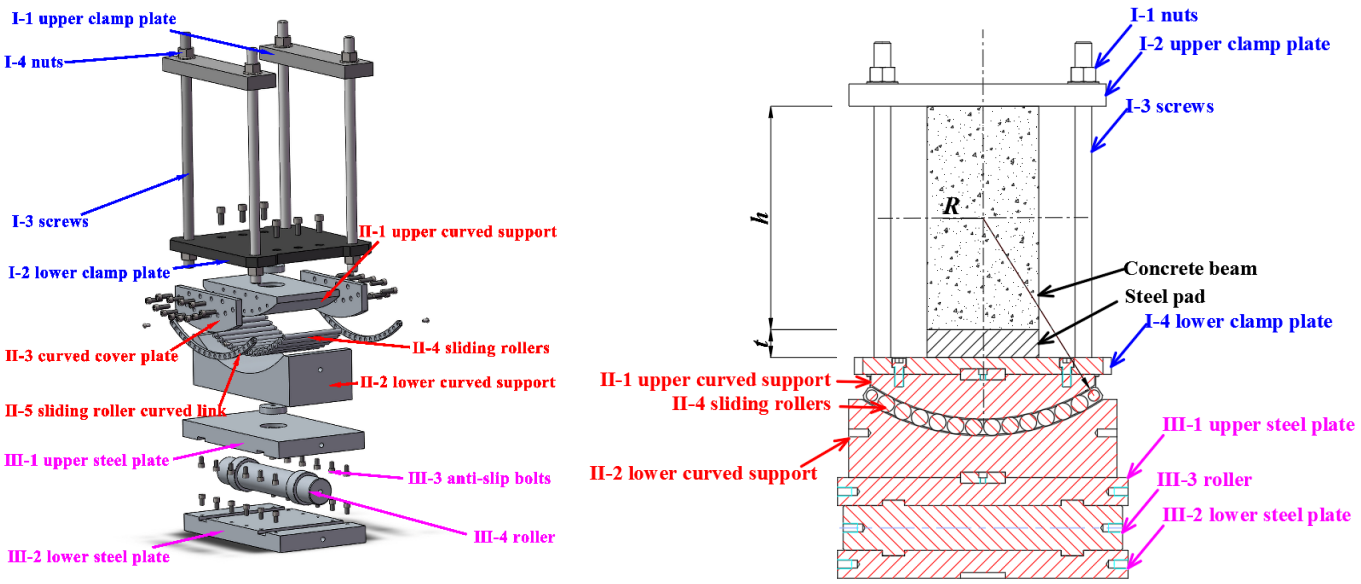

(**a**) (**b**)

Figure 4. Torsion support illustration: (**a**) 3D illustration; (**b**) cross-section.

2.4. Instrumentation

The strains in the longitudinal GFRP bars, GFRP stirrups, and concrete were measured by electrical resistance strain gauges (ERSGs) (as shown in Figure 5a). The ERSGs of longitudinal GFRP bars were located in the middle of the torsion span. The ERSGs of GFRP stirrups were installed in the middle of four legs of each stirrups. The ERSGs on the surface of the concrete were placed at 0°, 45°, and 90° to the specimen axis in a rosette shape to measure the local concrete strain state. The linear variable differential transformers (LVDTs) with an accuracy of 0.001 mm were mounted on the surface of the concrete surface. Inclinators with an accuracy of 0.01° were mounted at the top of specimens to measure the twist angle of specimens (as shown in Figure 5b). For the DIC measurement, a camera was employed to capture images of a 400 mm × 400 mm area at the middle of the torsion span on the north side of the specimens.

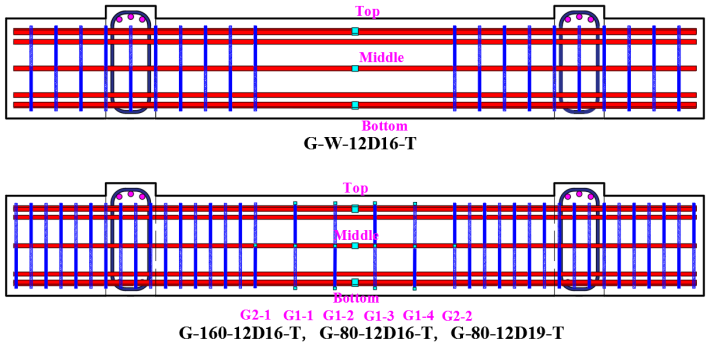

(**a**)

Figure 5. *Cont.*

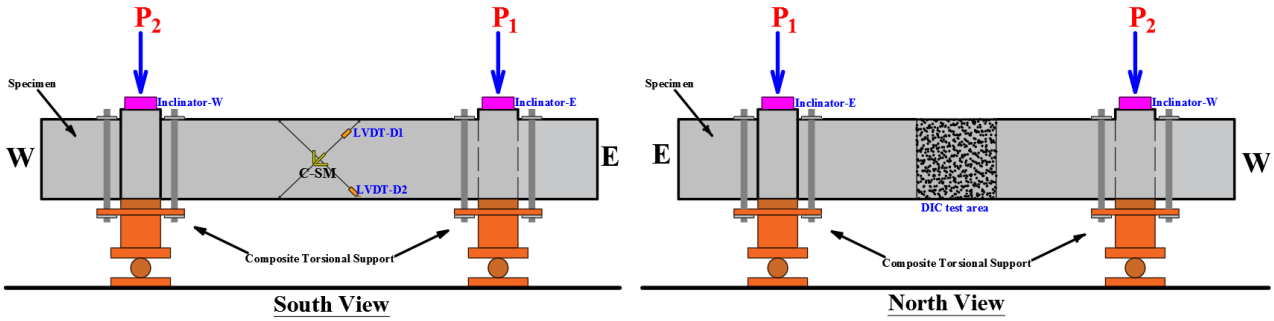

(**b**)

Figure 5. Instrumentation: (**a**) instrumentation in GFRP reinforcement; (**b**) instrumentation on the surface of specimens.

3. Results and Discussion

3.1. Overall Responses and Failure Patterns

Throughout the entire test process, no micro-cracks or local concrete crushing was observed in the anchorage zone or on the overhanging arms. The damage of all specimens was concentrated and developed at the test section. Based on the observation of concrete cracking, concrete crushing, and reinforcement behavior, the overall response and failure patterns can be summarized as follows:

1. The specimen without stirrups (G-W-12D16-T) experienced two stages: the uncracked stage and the failure stage. In the uncracked stage, the specimen exhibited visible warping on the surface. When the torque load reached cracking torque, diagonal cracks initiated from the mid-point of two long side surfaces, due to the maximum shear stress at these points. The crack rapidly extended from the midpoint to the top and bottom surfaces of the specimen, forming spiral cracks. With the increase in the width of the cracks on a randomly chosen long side surface of the specimen, the crack opening became significant. Simultaneously, a compressed plastic zone of concrete formed on the other long side surface of the specimen. Meanwhile, the spiral cracks extended to the corners of the specimen, where concrete spalling occurred. Generally, the specimen without stirrups failed immediately after cracking, which exhibited brittle failure as shown in Figure 6a.
2. The specimen with stirrups experienced three stages: pre-cracking stage, cracking stage, and failure stage. Specimens with stirrups exhibited similar behavior in the pre-cracking stage to the specimen without stirrups. In the pre-cracking stage, visible warping was also observed. When the torque load reached cracking torque, diagonal cracks first appeared at the midpoint of long side surfaces. The cracks extended towards the top and bottom surfaces of the specimen, forming spiral cracks on four side surfaces. As the load increased, the number of spiral cracks increased, and the crack width widened. Concrete inclined struts formed between the spiral cracks. In the failure stage, specimen G-160-12D16-T failed due to stirrup rupturing (as shown in Figure 6b), that is, a partially over-reinforced failure pattern. Specimens G-80-12D16-T and G-80-12D19-T failed due to the crushing of concrete strut (as shown in Figure 6c,d), that is, an over-reinforced failure pattern. The cracks on the over-reinforced specimens could be classified into two types: spiral cracks and intersected cracks (as shown in Figure 6c,d). Spiral cracks primarily formed due to torsion stress on the specimen, while intersected cracks primarily occurred due to the crushing of concrete struts.

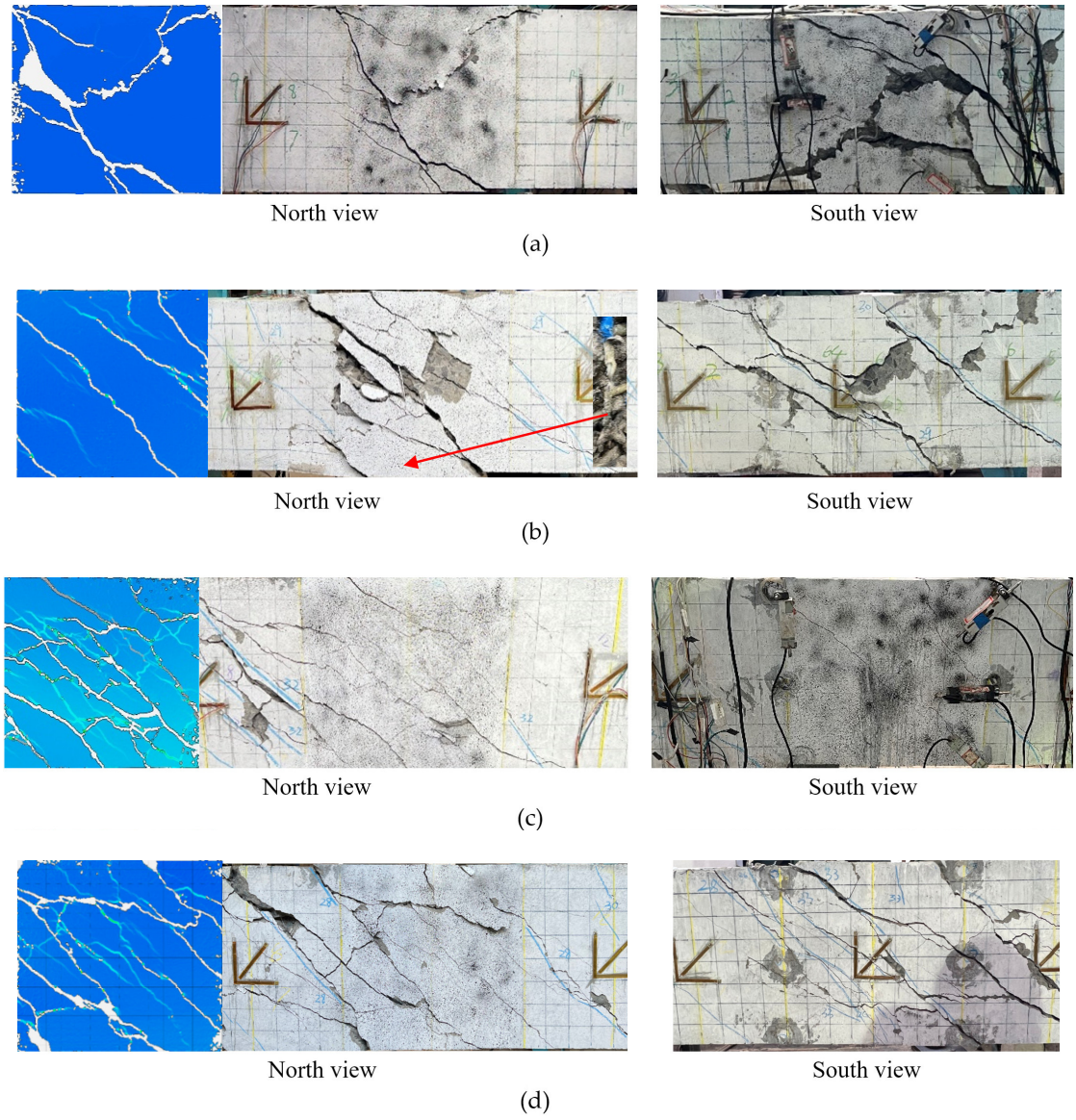

Figure 6. Cracking patterns of specimens at failure: (**a**) G-W-12D16-T; (**b**) G-160-12D16-T; (**c**) G-80-12D16-T; (**d**) G-80-12D19-T.

3.2. Spiral Crack Angle

In terms of spiral crack angle, the spiral crack angle is categorized into two types, as shown in Figure 7: (1) The tangent angle of the spiral crack at the mid-section of the specimen (referred to as the "tangent angle"), and (2) the angle of a straight line between two intersection points between crack and beam edge (referred to as the "secant angle"). The observation reveals the features as follows.

1. For specimens without stirrups, the tangent angle was approximately 45.9°, while the secant angle was 31.8°. After cracking, due to lack of stirrups confinement, the cracks extended longitudinally along the axis of the specimen, resulting in a secant angle smaller than the tangent angle.
2. For specimens with stirrups, the tangent angle was 45.1°, 43.8°, 45.1° for G-160-12D16-T, G-80-12D16-T, and G-80-12D19-T, respectively, and the secant angle ranged from 42.6°, 43.2°, and 46.2° for G-160-12D16-T, G-80-12D16-T, and G-80-12D19-T, respectively. For G-160-12D16-T, which failed due to stirrup rupturing, the axial elongation and crack width were larger than the other two specimens. It resulted in a

slightly smaller of secant angle to the tangent angle. Comparatively, two angles were close to each other for over-reinforced beams, G-80-12D16-T and G-80-12D19-T. All in all, the angle difference was much smaller than that in the beam without stirrups. It can be attributed to the constrain of FRP stirrups.

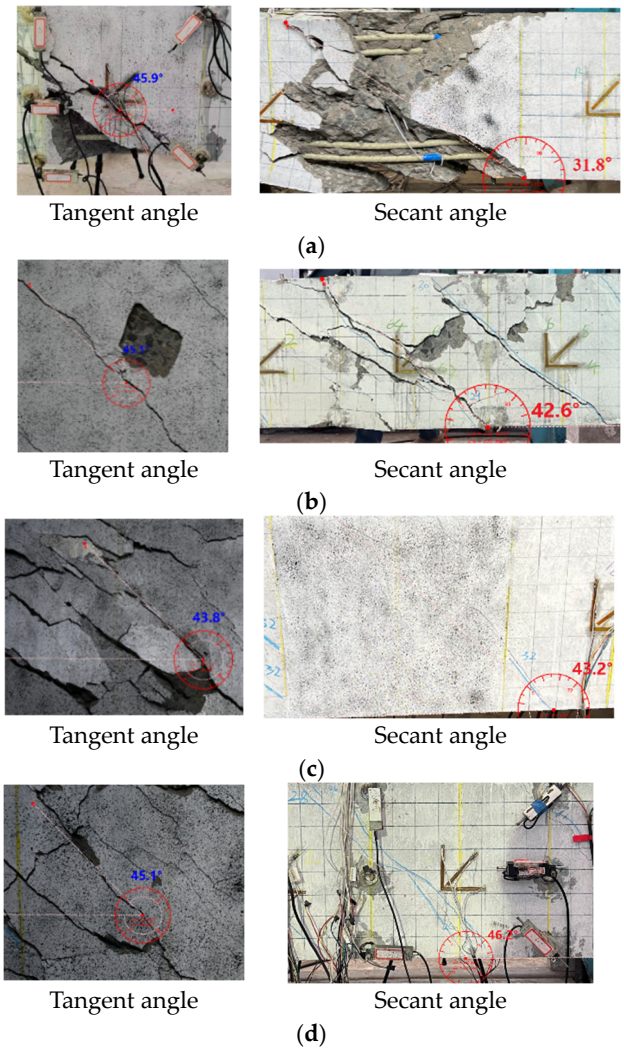

Figure 7. Spiral crack angle: (**a**) G-W-12D16-T; (**b**) G-160-12D16-T; (**c**) G-80-12D16-T; (**d**) G-80-12D19-T.

3.3. Crack Width

The torque–crack width curves of the specimen with stirrups are shown in Figure 8. The features of crack width development can be summarized as follows:

1. Generally, torque–crack width curves showed a rapid increase in crack width after cracking. For the same load, specimen G-160-12D16-T exhibited the widest crack width, while specimens G-80-12D19-T and G-80-12D16-T had smaller crack width. It indicated that the stirrups had a significant influence on the crack width, while the longitudinal reinforcement ratio had a lesser effect.
2. Corresponding to the crack width of 0.5 mm, torques were 23.5 kN·m for specimen G-160-12D16-T, 24.6 kN·m for G-80-12D16-T, and 24.3 kN·m for G-80-12D19-T, respectively. The ratios of the ultimate torque to the torque corresponding to 0.5 mm crack width were 1.09, 1.13, and 1.16, for G-160-12D16-T, G-80-12D16-T, and G-80-12D19-T, respectively. It indicated that the torque corresponding to 0.5 mm crack width was close to torsion capacity, with safety margins ranging from 1.1 to 1.2. Due to the different mechanisms of shear crack formation compared to flexural crack, the shear crack width of FRP-RC members subjected to torsion should be further investigated.

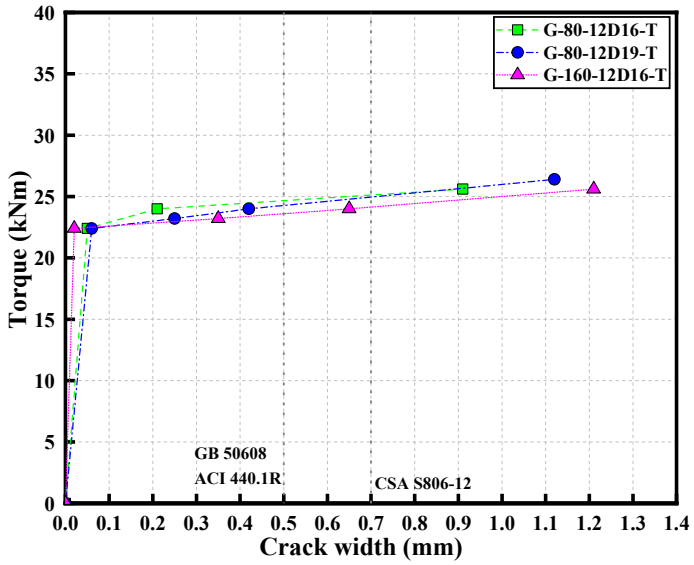

Figure 8. Torque–crack width curves.

3.4. Torque–Twist Angle Behavior

The torque–twist curves of the specimen without stirrups (G-W-12D16-T), the partially over-reinforced specimen (G-160-12D16-T), and the over-reinforced specimens (G-80-12D16-T and G-80-12D19-T) were shown in Figure 9. The features of the torque–twist angle curves of GFRP-RC beams can be summarized as follows:

1. Approximate linear torque–twist angle curves of the specimen without stirrups could be observed. The torque–twist angle behavior has no significant change after cracking. For the partially over-reinforced and over-reinforced specimens, the torque–twist angle curves exhibited bilinear characteristics. In the uncracked stage, the torque increased linearly with the twist until the cracking torque. Afterward, the torque–twist angle curves came into the cracking stage, with the torque increasing slowly until reaching the ultimate torque T_u. After reaching the ultimate torque, the torque–twist angle curves dropped rapidly. The torque–twist angle curves could be divided into three stages: uncracked stage, cracking stage, and failure stage. Similar torque–twist angle behavior of specimens with stirrups was displayed in References [8,10].
2. In terms of torsion capacity, for specimens with the same longitudinal reinforcement ratio, the ultimate torques (i.e., torsion capacity) T_u for G-W-12D16-T, G-160-12D16-T, and G-80-12D16-T were 24.9 kN·m, 25.6 kN·m, and 27.8 kN·m, respectively (as listed in Table 3). As the stirrup ratio increased from 0 to 0.98%, it increased by 12%. It indicated that increasing the stirrup ratio had a certain effect on enhancing the torsion capacity for partially over-reinforced beams. Besides, for over-reinforced specimens with the same stirrup ratio, the torsion capacity was 27.8 kN·m and 28.3 kN·m for specimens G-80-12D16-T and G-80-12D19-T, respectively (listed in Table 3). As the longitudinal reinforcement ratio increased from 3.01% to 4.25%, the torsion capacity increased by 2%, indicating that increasing the longitudinal reinforcement ratio for over-reinforced beams had a less significant effect on enhancing the torsion capacity of over-reinforced specimens.
3. In terms of ultimate twist angle, for the specimen without stirrups G-W-12D16-T, partially over-reinforced specimen G-160-12D16-T, and over-reinforced specimens G-80-12D16-T and G-80-12D19-T, the ultimate twist angles ϕ_u were 0.0018 rad/m, 0.0083 rad/m, 0.0403 rad/m, and 0.0244 rad/m, respectively (as listed in Table 3). For specimens with the same longitudinal reinforcement ratio, increasing the stirrup ratio from 0 to 0.98% resulted in a 21-fold increase in the ultimate twist angle. Increasing the stirrup ratio from 0.49% to 0.98% resulted in a 4.9-fold increase in the ultimate twist angle. It revealed that increasing the stirrup ratio could improve the torsional

deformation capacity significantly. It could be attributed confinement effect from stirrups. For over-reinforced specimens with the same stirrup ratio, increasing the longitudinal reinforcement ratio from 3.01% to 4.25% (an increase of 41%) resulted in a decrease in the ultimate twist angle from 0.0403 rad/m to 0.0244 rad/m (a decrease of 39%). It could be attributed to the dowel effect from the longitudinal bars during the twist.

4. In terms of torsional stiffness, the torsional stiffness in the torque–twist angle curves could be divided into pre-cracking torsional stiffness K_{un} and post-cracking torsional stiffness K_{cr}. The pre-cracking torsional stiffness and post-cracking torsional stiffness can be calculated by Equation (1) and Equation (2), respectively. The pre-cracking torsional stiffness for specimens G-W-12D16-T, G-160-12D16-T, G-80-12D16-T, and G-80-12D19-T were 13,833 kN·m^2, 14,500 kN·m^2, 9269 kN·m^2, and 12,294 kN·m^2, respectively, with an average pre-cracking torsional stiffness of 12,474 kN·m^2 (as listed in Table 3). The variation in pre-cracking torsional stiffness among the four specimens was within 26% of the average value, indicating that the pre-cracking torsional stiffness was significantly influenced by the concrete. For specimens with stirrups, the post-cracking torsional stiffness was 359 kN·m^2, 98 kN·m^2, and 326 kN·m^2 for G-160-12D16-T, G-80-12D16-T, and G-80-12D19-T respectively, which were 2%, 1%, and 3% of their pre-cracking torsional stiffness. In Reference [8] the post-cracking torsional stiffness decreased significantly, which ranged from 1% to 3% of their pre-cracking torsional stiffness.

$$K_{un} = \frac{T_{cr}}{\phi_{cr}} \text{ (Uncracked stiffness)} \quad (1)$$

$$K_{cr} = \frac{T_u - T_{cr}}{\phi_u - \phi_{cr}} \text{(Crack stiffness)} \quad (2)$$

5. In terms of ductility index, the ratio Δ of the ultimate twist angle ϕ_u to the cracking twist angle ϕ_{cr} (ϕ_u/ϕ_{cr}) was proposed to reflect the ductility index of FRP-RC beams. The ductility index can be calculated by Equation (3). The ductility indices for the over-reinforced specimens (G-80-12D16-T and G-80-12D19-T) were 15.5 and 14.4, respectively, with an average ductility index of 14.9 (as listed in Table 3). The longitudinal reinforcement ratio had little effect on the ductility index of over-reinforced specimens. The ductility indices Δ for the specimen without stirrups G-W-12D16-T, the partially over-reinforced specimen G-160-12D16-T, and the over-reinforced specimens (G-80-12D16-T and G-80-12D19-T) were 1.0, 5.2, and 14.9, respectively. The ductility indices of the partially over-reinforced specimen G-160-12D16-T and the over-reinforced specimen G-80-12D16-T were approximately 5 times and 15 times that of the specimen without stirrups G-W-12D16-T, respectively. It indicated that increasing the stirrup ratio could improve the deformation capacity of GFRP-RC beams significantly. Over-reinforced specimens had better ductility than specimens with the other two failure patterns.

$$\Delta = \frac{\phi_u}{\phi_{cr}} \quad (3)$$

Table 3. Summary of test results.

Specimens	ϕ_{cr} (Rad/m)	ϕ_u (Rad/m)	ϕ_u/ϕ_{cr}	T_{cr} (kN·m)	T_u (kN·m)	K_{un} (kN·m^2)	K_{cr} (kN·m^2)	Failure Pattern
G-W-12D16-T	0.0018	0.0018	1.0	24.9	24.9	13,833	-	Concrete Cracking
G-160-12D16-T	0.0016	0.0083	5.2	23.2	25.6	14,500	359	Stirrup Rupturing
G-80-12D16-T	0.0026	0.0403	15.5	24.1	27.8	9269	98	Concrete Crushing
G-80-12D19-T	0.0017	0.0244	14.4	20.9	28.3	12,294	326	Concrete Crushing

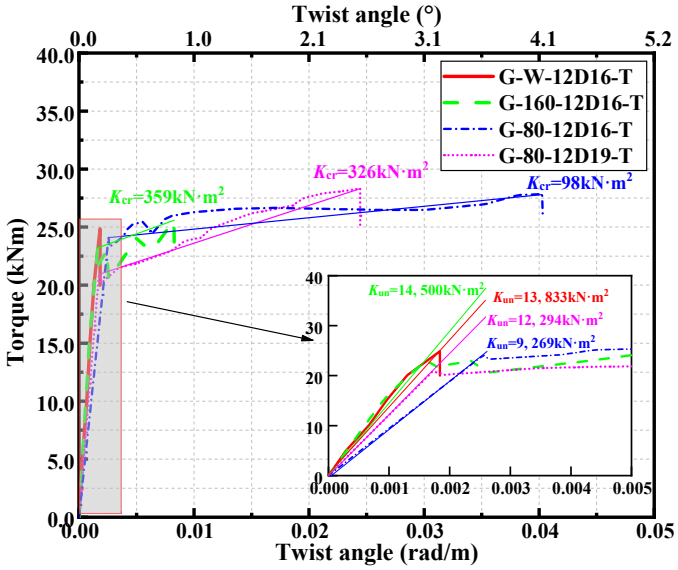

Figure 9. Torque–twist angle curves.

3.5. Strains in Longitudinal Reinforcement

The torque–longitudinal reinforcement strain curves are shown in Figure 10. Strain gauges were concentrated at the upper, middle, and lower longitudinal reinforcement in the mid-span of the specimens. The features of the torque–longitudinal reinforcement strain curves for GFRP-RC beams can be summarized as follows:

1. In terms of specimens without stirrups (G-W-12D16-T), the longitudinal reinforcement strain increased with the torque before the concrete cracked. After cracking, the torque decreased rapidly, and the longitudinal reinforcement strain no longer increased. The longitudinal reinforcement strain corresponding to the ultimate torque was less than 100 με. It indicated that the contribution of the longitudinal reinforcement to the torsion capacity of the specimen without stirrups was weak. Additionally, there were little differences in the strain of the top, middle, and bottom longitudinal reinforcement, indicating that the longitudinal reinforcements at the top, middle, and bottom were in a similar stress state.
2. In terms of specimens with stirrups (G-160-12D16-T, G-80-12D16-T, and G-80-12D19-T), they exhibited different performance in torque–longitudinal reinforcement strain curves. Before cracking, the longitudinal reinforcement strain was less than 100 με. After cracking, the longitudinal reinforcement strain suddenly increased and slowly continued to increase up to the ultimate torque. This showed that before cracking, the axial tension in the longitudinal reinforcement was relatively low. After cracking, there was a redistribution of internal stresses within the specimen, forming a new load transfer mechanism among the longitudinal reinforcement, stirrups, and concrete, leading to the sudden increase in longitudinal reinforcement strain.
3. For specimen G-160-12D16-T, the average longitudinal reinforcement strains corresponding to ultimate torque were 863 με. For specimens G-80-12D16-T and G-80-12D19-T, the average longitudinal reinforcement strains corresponding to ultimate torque were 3018 με and 2042 με, respectively. It revealed that longitudinal reinforcement could provide sufficient tension force sustainably for partially over-reinforced specimens and over-reinforced specimens to form truss mode with longitudinal reinforcement, stirrup, and concrete structures. Comparing partially over-reinforced specimens and over-reinforced specimens, increasing the stirrup ratio could improve the torsion capacity. Higher torsion capacity resulted in more strains in longitudinal reinforcement. In comparison between G-80-12D16-T and G-80-12D16-T, the force transferred by the truss model in longitudinal reinforcement was similar, the average

strain of G-80-12D16-T was higher than that of G-80-12D19-T due to smaller area of longitudinal reinforcement in G-80-12D16-T.

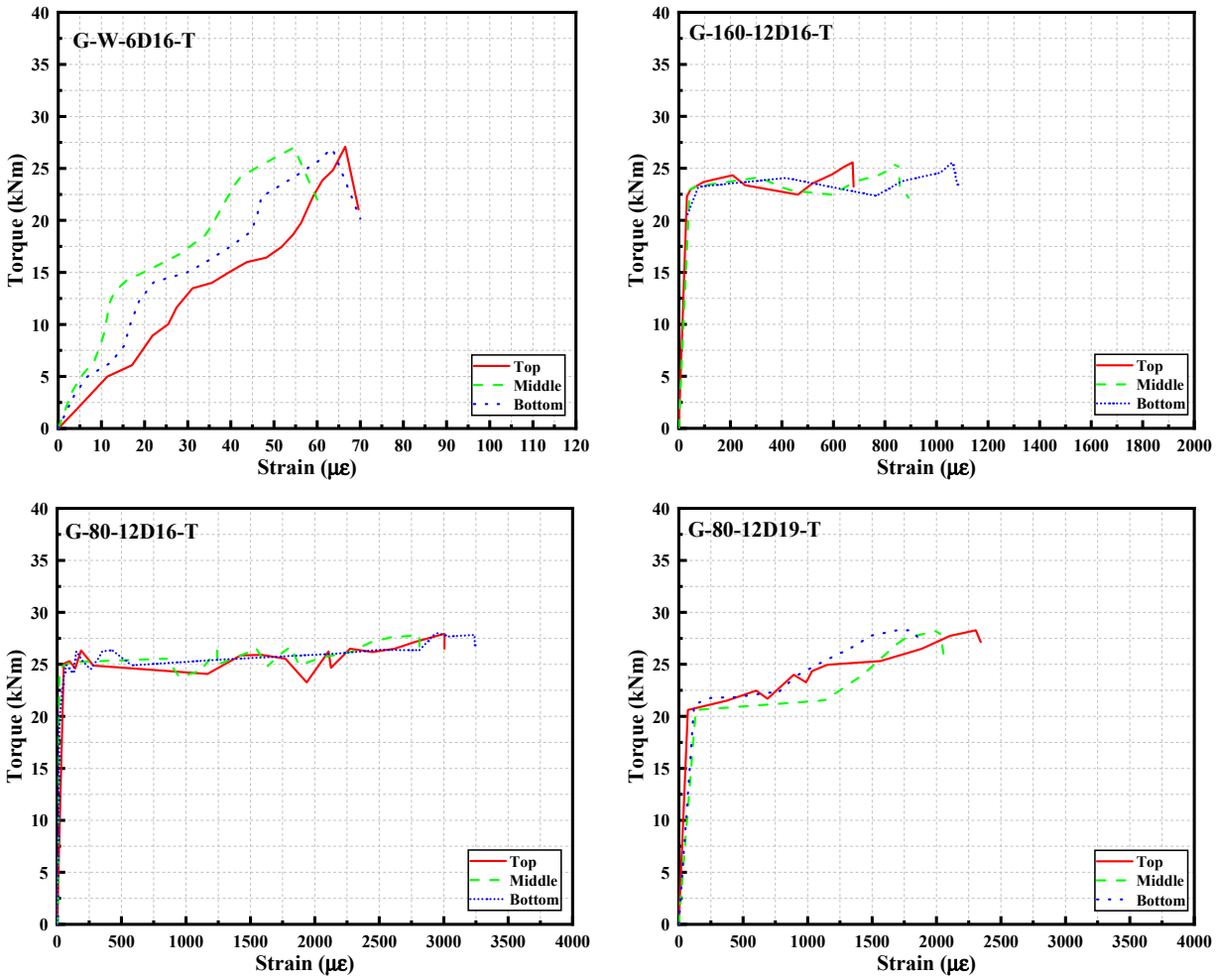

Figure 10. Torque–longitudinal reinforcement strain curves.

3.6. Strains in Transversal Reinforcement

The torque–stirrup strain curves for specimens G-160-12D16-T, G-80-12D16-T, and G-80-12D19-T were shown in Figure 11. The features of the torque–stirrup strain curves can be summarized as follows:

1. Generally, the torque–stirrup strain curves for the specimens G-160-12D16-T, G-80-12D16-T, and G-80-12D19-T exhibited similar behavior. Before concrete cracking, the stirrup strains were relatively small. After concrete cracking, the stirrup strains increased rapidly until they reached the ultimate torque. It indicated that the GFRP stirrups played a minor role before concrete cracking. However, after cracking, the GFRP stirrups could provide a certain enhancement to the torsion behavior of GFRP-RC beams.
2. To compare the strains in different specimens, the average stirrup strain was approximately 3341 με with a standard deviation of 2131 με for specimen G-160-12D16-T. For specimen G-80-12D16-T, the average stirrup strain was approximately 4577 με with a relatively smaller standard deviation of 1664 με. For specimen G-80-12D19-T, the average stirrup strain was approximately 3364 με with a similar standard deviation of 1488 με. The strain distribution in the stirrups of over-reinforced specimens was less dispersed compared to partially over-reinforced specimens. This was mainly because the crack spacing in over-reinforced specimens was smaller than that in partially

over-reinforced specimens, leading to more uniform tensile stress distribution across the stirrup legs in the partially over-reinforced specimen.

3. To compare the strains in short and long stirrup legs, the ratio between strain in the short legs to the strain in the long legs of the GFRP stirrups in the middle of the test section was 0.39, 0.39, and 0.4 for specimen G-160-12D16-T, G-80-12D16-T, and G-80-12D19-T, respectively. Different from only long legs of stirrups cross the diagonal crack appeared in the beams under shear, both the short and long legs of stirrups were intersected by the spiral cracks in beams and participated in torsion resistance.
4. The strain in the long leg of the ruptured stirrup was approximately 7600 με corresponding to 426 MPa, which was $0.88 \cdot f_{bend,exp}$, and $0.39 \cdot f_{fu}$. It indicated that $0.4 \cdot f_{fu}$ specified in CSA S806-12 proved to be reasonable for torsion design, while the stirrup strain limit 4000 με in CSA S9-6:19 and AASHTO GFRP-RC 2018 appeared to be conservative. In this study, the stirrup strain limit was regarded as the average of the ultimate strains of all stirrups that intersected the critical crack for all specimens. The stirrup strain limit of 5200 με was suggested for torsion design. However, due to limited test data, the stirrup strain limit should be further investigated.

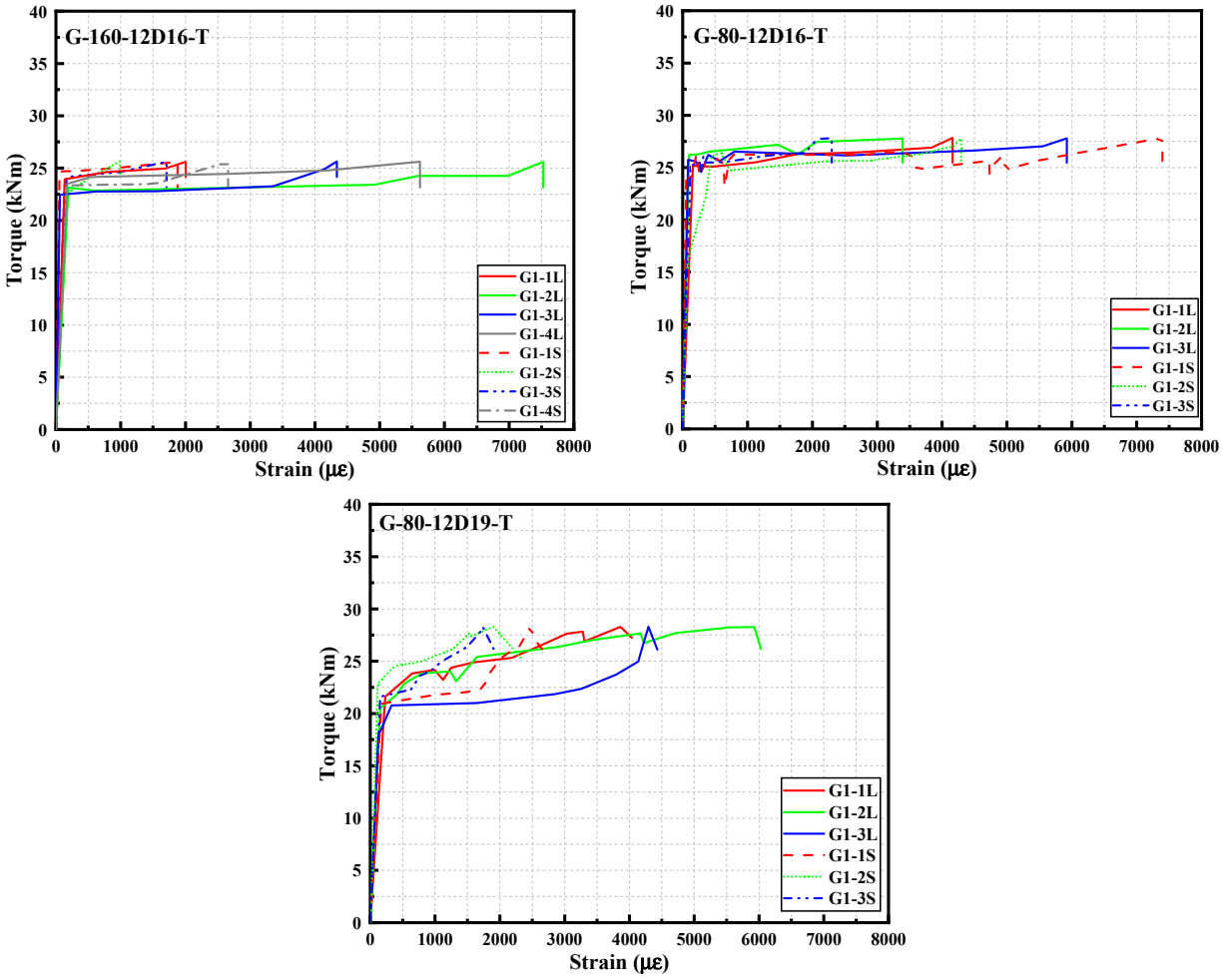

Figure 11. Torque–transverse reinforcement strain curves.

3.7. Concrete Strain

The torque–concrete strain curves (directions: 0-degree, 45-degree, 90-degree, and 135-degree) were illustrated in Figure 12. The features of the torque–concrete strain curves can be summarized as follows:

1. In terms of concrete strains in 0-degree, 45-degree, and 90-degree directions, the torque–concrete strain curves for specimen without stirrups (G-W-12D16-T) and specimen

with stirrups (G-160-12D16-T, G-80-12D16-T, and G-80-12D19-T) exhibited similar behavior. In all three directions, the concrete strain increased linearly with torque. The concrete strain in the 0-degree and 90-degree directions was below 50 με. The concrete strain in the 45-degree direction was approximately 200 με. Calculated with concrete strain in 0-degree, 45-degree, and 90-degree directions, the principle stress angle was about 45° for all specimens. It indicated that the surfaces of the specimens were under a pure shear stress state. The testing setup effectively achieved a pure torsion loading mode for the specimens.

2. In terms of concrete strains in a 135-degree direction, for the specimen without stirrups, the compressive strain was below 200 με because of concrete cracking failure. For the partially over-reinforced specimen G-160-12D16-T, the compressive strain in the concrete at the ultimate torque was approximately 900 με. In contrast, for the over-reinforced specimens G-80-12D16-T and G-80-12D19-T, the compressive strain in the concrete at the ultimate torque was approximately 1500 με and 1200 με, respectively, with an average of 1350 με, which was 1.5 times the compressive strain at the ultimate torque for the partially over-reinforced specimen.

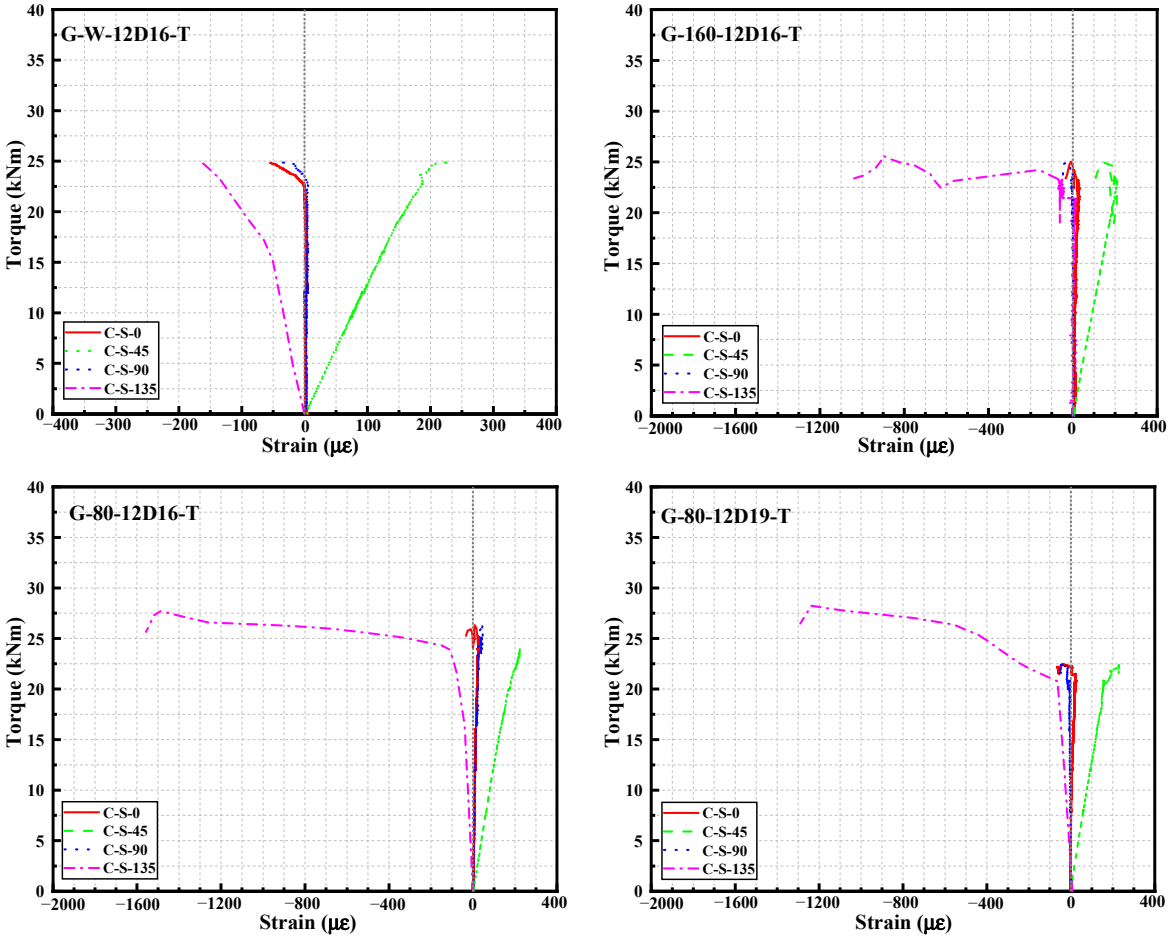

Figure 12. Torque–concrete strain curves.

4. Evaluation of Torsion Design Equations and Design Suggestions

4.1. Evaluation of Torsion Capacity Equations

In terms of the calculation of torsion capacity, the equations were proposed to calculate the torsion capacity for partially over-reinforced FRP-RC beams. For over-reinforced FRP-RC beams, the cross-sectional limit conditions were used to avoid concrete crushing. Available torsion capacity equations from codes CSA S806-12, CSA S6: 19, AASHTO GFRP-

RC 2018, and ACI 440.11-22 were based on the space truss model to calculate torsion capacity of FRP-RC members which failed due to stirrup rupturing.

$$T_u = 2A_0 \cdot \frac{A_{ft1} f_{ft}}{s} \cdot \cot\theta \quad (4)$$

where A_0 referred to the area enclosed by the shear flow centerline; A_{ft1} represented the cross-sectional area of one leg of the stirrup; and f_{ft} represented the tensile strength of FRP stirrups. θ represented the crack angle and s was stirrup spacing.

In this study, four codes, including CSA S806-12, CSA S6: 19, AASHTO GFRP-RC 2018, and ACI 440.11-22, for calculating the torsion capacity of FRP-PC members were considered. To assess the performance of the torsion capacity equations in the above four design guidelines, a database of 32 FRP-RC beams with stirrups was collected from references [8–10,27] to establish a test database of FRP-RC beams under torsion. Of the 32 FRP-RC beams, 19 beams failed due to stirrup rupturing, and 13 beams failed due to concrete crushing. The database information and ratio between the experimental and predicted torsion capacity T_{exp}/T_{pre} are listed in Table 4. All material reduction and safety factors were set equal to 1.0. The crack angle θ was taken as 45°. Table 5 presents the torsion capacity ratio T_{exp}/T_{pre}. The features of the torsion capacity ratio from different codes can be summarized as follows:

1. Generally, the four codes underestimated the torsion capacity of FRP-RC beams. However, CSA S806-12 based on modified compression field theory provided the most accurate predictions with a mean of T_{exp}/T_{pre} 1.48 and a standard deviation of 0.48. It could be attributed that the tensile strength of the FRP stirrup was regarded as $0.4 f_{fu}$ which was greater than $\varepsilon_{lim} \cdot E_f$. The stirrup strain limit ε_{lim} was regarded as 4000 με for CSA S6-19 and AASHTO. and 5000 με for ACI 440.11-22.
2. In terms of failure pattern, all codes provided the more conservative predictions for stirrup rupturing failure with a mean of T_{exp}/T_{pre} over 1.95 compared to the predictions for concrete crushing failure. Particularly, CSA S806-12 provided an unsafety prediction with a mean of T_{exp}/T_{pre} of 0.80. It indicated that the design equations in four codes should be used to calculate the torsion capacity of FRP-RC beams which failed due to stirrup rupturing.
3. CSA S6: 19 provided the most conservative predictions with a mean of T_{exp}/T_{pre} of 3.59. The tensile strength of stirrups specified in CSA S6: 19 was calculated by $\varepsilon_{lim} \cdot E_f$. Additionally, A_0 was 0.85 times the area enclosed by the centerline of the stirrup. The concrete cover was disregarded to calculate the A_0.
4. CSA S6-19, AASHTO, and ACI 440.11-22 underestimated the torsion capacity of the AFRP-RC beam obviously, with a mean of T_{exp}/T_{pre} over 6.18. Especially, the underestimation of torsion capacity occurred in AFRP-RC beams that failed due to stirrup rupturing. The E_f of AFRP bars was similar to that of GFRP bars. However, the f_{fu} of the AFRP bar was about 2 times of the GFRP bars. However, ε_{lim} was used to calculate the tensile strength of stirrups in CSA S6-19, AASHTO, and ACI 440.11-22. The ε_{lim} was underestimated in calculating the torsion capacity of AFRP-RC beams.

Table 4. Comparisons between the experimental and predicted torsion capacity of FRP-RC beams.

Reference	Specimen	h (mm)	b (mm)	ρ_t (%)	Stirrup	Failure Pattern	$T_{u,exp}$ (kN·m)	$T_{u,exp}/T_{u,pre}$			
								CSA S806-12	CSA S6: 19	AASHTO GFRP-RC	ACI 440.11-22
Reference [8]	BG120	600	250	0.47	GFRP	SR	52.7	1.51	3.19	3.01	2.55
	BG180	600	250	0.31	GFRP	SR	41.8	1.79	3.79	3.58	3.03
	BG240	600	250	0.24	GFRP	SR	34.2	1.95	4.14	3.90	3.31
	BG300	600	250	0.19	GFRP	SR	29.9	2.14	4.52	4.27	3.62

Table 4. *Cont.*

Reference	Specimen	h (mm)	b (mm)	ρ_t (%)	Stirrup	Failure Pattern	$T_{u,exp}$ (kN·m)	$T_{u,exp}/T_{u,pre}$			
								CSA S806-12	CSA S6: 19	AASHTO GFRP-RC	ACI 440.11-22
Reference [10]	BC120	600	250	0.47	CFRP	SR	62.9	1.09	1.31	1.24	1.05
	BC180	600	250	0.31	CFRP	SR	49.4	1.29	1.55	1.46	1.24
	BC240	600	250	0.24	CFRP	SR	39.4	1.37	1.64	1.55	1.31
	BC300	600	250	0.19	CFRP	SR	35.7	1.55	1.86	1.75	1.49
Reference [9]	BG60	600	250	0.94	GFRP	CC	56.9	0.81	1.72	1.62	1.38
	BC60	600	250	0.94	CFRP	CC	69.3	0.60	0.72	0.68	0.58
Reference [27]	AFRP	150	115	1.91	AFRP	CC	3.7	0.51	1.26	0.77	1.00
	CFRP	150	115	1.91	CFRP	CC	4.4	0.51	0.52	0.32	0.41
	A1	220	140	0.26	AFRP	SR	8.0	2.10	7.36	6.13	5.89
	A2	220	140	0.27	AFRP	SR	7.2	1.84	6.45	5.20	5.16
	A3	220	140	0.26	AFRP	SR	9.2	2.39	8.38	6.99	6.71
	A4	220	140	0.26	AFRP	SR	8.3	2.16	7.60	6.33	6.08
	A5	220	140	0.26	AFRP	SR	10.1	2.62	9.21	7.67	7.37
	A6	220	140	0.27	AFRP	SR	10.4	2.67	9.38	7.57	7.51
	A7	220	140	0.26	AFRP	SR	11.5	2.99	10.48	8.74	8.38
	A8	220	140	0.27	AFRP	SR	10.4	2.67	9.36	7.56	7.49
	C1	220	140	1.20	CFRP	CC	10.0	0.53	0.82	0.64	0.65
	C2	220	140	0.84	CFRP	CC	9.2	0.69	1.07	0.83	0.85
	C3	220	140	1.01	CFRP	CC	10.0	0.77	1.08	0.87	0.87
	C4	220	140	0.37	CFRP	SR	8.7	1.81	2.57	2.07	2.05
	C5	220	140	0.84	CFRP	CC	13.6	1.01	1.57	1.22	1.25
	C6	220	140	1.20	CFRP	CC	14.7	0.77	1.20	0.93	0.96
	C7	220	140	1.01	CFRP	CC	12.3	0.94	1.32	1.07	1.06
	C8	220	140	0.37	CFRP	SR	10.5	2.20	3.11	2.51	2.49
	C9	220	140	1.20	CFRP	CC	12.8	0.67	1.04	0.81	0.83
This study	G-160-12D16-T	400	200	0.49	GFRP	SR	25.6	0.88	1.73	1.42	1.39
	G-80-12D16-T	400	200	0.98	GFRP	CC	27.8	0.90	1.76	1.45	1.41
	G-80-12D19-T	400	200	0.98	GFRP	CC	28.3	1.63	3.19	2.62	2.56

Note: SR = stirrup rupturing; CC = concrete crushing.

Table 5. Statistics of torsion capacity ratio $T_{u,exp}/T_{u,pre}$.

Code	In Total (32 Beams)		SR (19 Beams)		CC (13 Beams)		GFRP-RC (8 Beams)		CFRP-RC (15 Beams)		AFRP-RC (9 Beams)	
	MEAN	SD	MEAN	SD	MEAN	SD	MEAN	SD	MEAN	SD	MEAN	SD
CSA S806-12	1.48	0.74	1.95	0.56	0.80	0.29	1.45	0.49	1.09	0.49	2.22	0.69
CSA S6: 19	3.59	3.07	5.14	3.11	1.33	0.64	3.01	1.07	1.48	0.66	7.72	2.56
AASHTO GFRP-RC	3.02	2.54	4.37	2.49	1.06	0.56	2.73	1.07	1.23	0.57	6.33	2.19
ACI 440.11-22	2.87	2.46	4.11	2.49	1.06	0.52	2.41	0.85	1.18	0.53	6.18	2.04

Note: SR = stirrup rupturing; CC = concrete crushing; SD = standard deviation.

4.2. Design Suggestions

Based on the collected data from References [8–11] of FRP-RC beams with stirrups under torsion, this study examined the spiral crack angles (tangent angle and secant angle) as depicted in Figure 13. It showed the ratio of ρ_t/ρ_l influenced the spiral crack angle of specimens with stirrups, insignificantly. Statistically, the average tangent angle was 45° with a standard deviation of 0.5, and the average secant angle was 44.2° with a standard deviation of 1.5. Additionally, design codes such as ACI 318-19 [28], EC 2 [29], and ACI 440.11-22 [22] specified using the spiral crack angle of 45 for calculating the torsion capacity. Therefore, the crack angle of 45° was suggested to calculate torsion capacity. Additionally, as mentioned above (Section 3.6), based on the test results, the stirrup strain limit of 5200 με was suggested for torsion design.

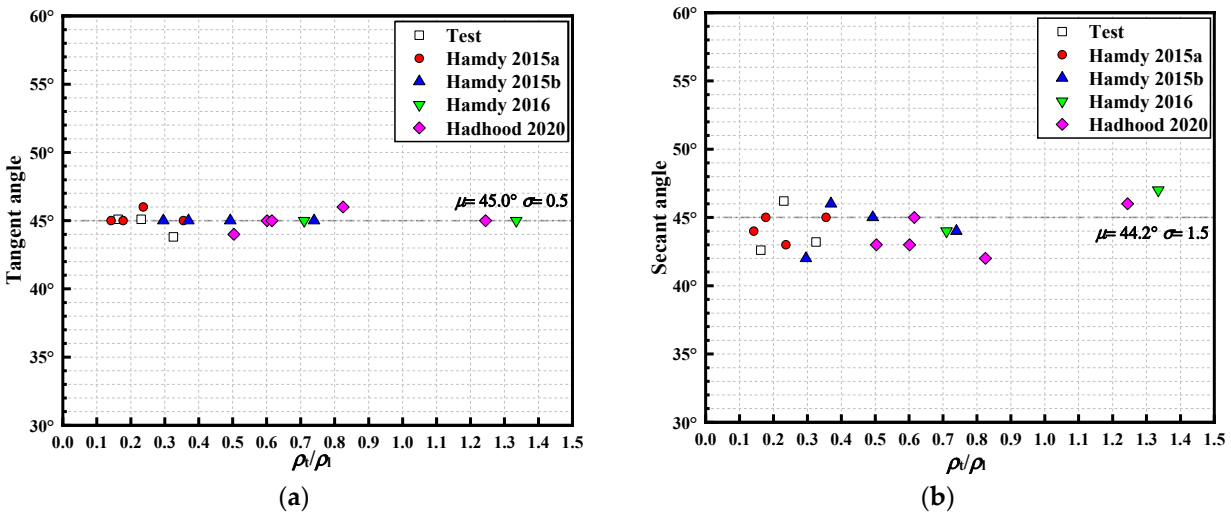

Figure 13. Spiral crack angle of FRP-RC beams with stirrups [8–11]: (**a**) tangent angle; (**b**) secant angle.

5. Conclusions

The four large-scale GFRP-RC beams (2800 mm × 400 mm × 200 mm) reinforced with symmetric longitudinal reinforcement were tested to investigate the influence of longitudinal and transverse reinforcement ratio on the torsion behavior. Based on the analysis of the experimental results, the following conclusions can be drawn:

1. Three typical torsion failure patterns were observed, that is, concrete cracking failure for specimen without stirrups, stirrup rupturing failure for partially over-reinforced specimens, and concrete crushing failure for over-reinforced specimens. The variation of failure patterns can be achieved by the variation of stirrup ratio.
2. Based on test data, the tangent angle of the spiral cracks was approximately 45°. The secant angle for specimens without stirrups was 31.8°, while the angle for specimens with stirrups ranges from 42°~47° with an average value of 44.2°.
3. For specimens with the same longitudinal reinforcement ratio, the torsion capacity of the specimen without stirrups, partially over-reinforced specimens and over-reinforced specimens was 24.9 kN·m, 25.6 kN·m, and 27.8 kN·m, respectively. When the stirrup ratio increased from 0 to 0.98%, the torsion capacity increased by 12%. For specimens with the same stirrup ratio, the torsion capacity was 27.8 kN·m and 28.3 kN·m for G-80-12D16-T and G-80-12D19-T, respectively. The longitudinal reinforcement ratio increased from 3.01% to 4.25%, showing an increase of only 1.8%.
4. For specimens with the same longitudinal reinforcement ratio, the ultimate twist angle ϕ_u of the specimen without stirrups (G-W-12D16-T), partially over-reinforced specimens (G-160-12D16-T) and over-reinforced specimens (G-80-12D16-T) was 0.0018 rad/m, 0.0083 rad/m and 0.0403 rad/m, respectively. The increase in the stirrup ratio could enhance the torsion deformation capacity significantly.

5. The longitudinal reinforcement strain in specimens without stirrups corresponding to ultimate torque was below 100 με, indicating that the axial tensile of the longitudinal reinforcement contributed to the torsion capacity insignificantly. The stirrups of partially over-reinforced specimens ruptured at the bend, with a rupture strain of approximately 7600 με.
6. Regarding the beams with stirrup rupturing failure, CSA S806-12 provided the most accurate predictions with a mean of T_{exp}/T_{pre} 1.95 and a standard deviation of 0.56. CSA S6: 19 provided the most conservative predictions with a mean of T_{exp}/T_{pre} of 5.14 and a standard deviation of 3.11. In terms of torsion design, the crack angle of 45° and stirrup strain limit of 5200 με were suggested.

Author Contributions: Conceptualization, W.X., J.J. and H.B.; methodology, J.J. and X.H.; software, H.B.; writing—original draft preparation, H.B.; writing—review and editing, W.X. and J.J.; funding acquisition, W.X. and J.J. All authors have read and agreed to the published version of the manuscript.

Funding: This research was funded by the National Key Research and Development Program of China (Grant No. 2022YFB3706500), the National Natural Science Foundation of China (Grant No. 52378178 & 52130806), and the Program Fund of Non-Metallic Excellence and Innovation Center for Building Materials (2023TDA4-1).

Data Availability Statement: The original contributions presented in the study are included in the article, further inquiries can be directed to the corresponding authors.

Acknowledgments: The authors gratefully acknowledge the financial support provided by National Key Research and Development Program of China, the National Natural Science Foundation of China and the Non-Metallic Excellence and Innovation Center for Building Materials.

Conflicts of Interest: The authors declare no conflicts of interest.

References

1. Nanni, A.; De Luca, A.; Zadeh, J. *Reinforced Concrete with FRP Bars Mechanics and Design*; CRC Press: New York, NY, USA, 2014; pp. 3–7.
2. Grace, N.; Jensen, A.; Eamon, D. Life-cycle cost analysis of carbon fiber-reinforced polymer reinforced concrete bridges. *ACI Struct. J.* **2012**, *109*, 697–704.
3. Eamon, C.D.; Jensen, E.A.; Grace, N.F. Life-cycle cost analysis of alternative reinforcement materials for bridge superstructures considering cost and maintenance uncertainties. *J. Mater. Civ. Eng.* **2012**, *24*, 373–380. [CrossRef]
4. Imjai, T.; Guadagnini, M.; Pilakoutas, K. Bend strength of FRP bars: Experimental investigation and bond modeling. *J. Mater. Civ. Eng.* **2017**, *29*, 04017024. [CrossRef]
5. Koutchoukali, N.-E.; Belarbi, A. Torsion of High-Strength Reinforced Concrete Beams and Minimum Reinforcement Requirement. *ACI Struct. J.* **2001**, *98*, 462–469.
6. Fang, I.-K.; Shiau, J.-K. Torsional Behavior of Normal- and High-Strength Concrete Beams. *ACI Struct. J.* **2004**, *101*, 304–313.
7. Thomas, T.C.H. Torsion of Structural Concrete A Summary on Pure Torsion. *ACI Symp. Pap.* **1968**, *18*, 165–178.
8. Hamdy, M.; Benmokrane, B. Torsion Behavior of Concrete Beams Reinforced with Glass Fiber-Reinforced Polymer Bars and Stirrups. *ACI Struct. J.* **2015**, *112*, 543–552.
9. Hamdy, M.; Benmokrane, B. Reinforced Concrete Beams with and without FRP Web Reinforcement under Pure Torsion. *J. Bridge Eng.* **2016**, *21*, 04015070.
10. Hamdy, M.; Omar, C.; Benmokrane, B. Torsional Moment Capacity and Failure Mode Mechanisms of Concrete Beams Reinforced with Carbon FRP Bars and Stirrups. *J. Compos. Constr.* **2015**, *19*, 04014049.
11. Hadhood, A.; Gouda, M.G. Torsion in concrete beams reinforced with GFRP spirals. *Eng. Struct.* **2020**, *206*, 110174. [CrossRef]
12. Xiong, H.; Li, B.; Jiang, J. Load path dependence of strain and stress for confined concrete. *Mag. Concr. Res.* **2016**, *68*, 604–618. [CrossRef]
13. Deifalla, A.; Hamed, M.; Saleh, A.; Ali, T. Exploring GFRP bars as reinforcement for rectangular and L-shaped beams subjected to significant torsion: An experimental study. *Eng. Struct.* **2014**, *59*, 776–786. [CrossRef]
14. Zhou, J.; Shen, W.; Wang, S. Experimental study on torsional behavior of FRC and ECC beams reinforced with GFRP bars. *Constr. Build. Mater.* **2017**, *152*, 74–81. [CrossRef]
15. Deifalla, A. Torsional Behavior of Rectangular and Flanged Concrete Beams with FRP Reinforcements. *J. Struct. Eng.* **2015**, *141*, 04015068. [CrossRef]
16. Mostafa, I.T.; Mousa, S.; Mohamed, H.M.; Benmokrane, B. Experimental and Analytical Behavior of GFRP-Reinforced Concrete Box Girders under Pure Torsion. *J. Compos. Constr.* **2024**, *28*, 04023064. [CrossRef]

17. Hu, X.; Xue, W.; Xue, W. Bond properties of GFRP rebars in UHPC under different types of test. *Eng. Struct.* **2024**, *314*, 118319. [CrossRef]
18. *CAN/CSA S6:19*; Canadian Highway Bridge Design Code (CAN/CSA S6:19). Canadian Standards Association: Rexdale, ON, Canada, 2019.
19. *ACI 440.1R-15*; Guide for the Design and Construction of Structural Concrete Reinforced with FRP Bars. ACI Committee: Farmington Hills, MI, USA, 2015.
20. *AASHTO GFRP-RC 2018*; Bridge Design Guide Specifications for GFRP-Reinforced Concrete. American Association of State Highway and Transportation Officials: Washington, DC, USA, 2018.
21. *GB 50608-2020*; Technical Standard for Fiber Reinforced Polymer (FRP) in Construction. China Planning Press: Beijing, China, 2020.
22. *ACI 440.11-22*; Building Code Requirements for Structural Concrete Reinforced with Glass Fiber Reinforced Polymer (GFRP) Bars-Code and Commentary. ACI Committee: Farmington Hills, MI, USA, 2023.
23. *CAN/CSA S806-12*; Design and Construction of Building Structures with Fibre-Reinforced Polymers. Canadian Standards Association: Mississauga, ON, Canada, 2012.
24. *GB/T 50081-2002*; Standard for Test Method of Mechanical Properties on Ordinary Concrete. China Building Industry Press: Beijing, China, 2002.
25. *ACI 440.3R-12*; Guide Test Methods for Fiber Reinforced Polymer Composites for Reinforcing or Strengthening Concrete and Masonry Structures. ACI Committee: Farmington Hills, MI, USA, 2012.
26. Xue, W.; Bai, H.; Hu, X.; Jiang, J. A Composite Torsion Test Loading Device of a Beam Member and a Test Method for Combined Action of Shear and Torsion. *Chinese Patent. CN202211595007.3.* 2022.
27. Razaqpur, A.G.; Bencardino, F.; Rizzuti, L.; Spadea, G. FRP reinforced/prestressed concrete members: A torsion design model. *Compos. Part B Eng.* **2015**, *79*, 144–155. [CrossRef]
28. *ACI 318-19*; Building Code Requirements for Structural Concrete Commentary on Building Code Requirements for Structural Concrete. ACI Committee: Farmington Hills, MI, USA, 2019.
29. *EN 1992-1-1*; Eurocode 2: Design of Concrete Structures- Part 1-1: General Rules and Rules for Buildings. European Committee for Standardization: Brussels, Belgium, 1992.